Relating Charge Transport, Contact Properties, and Recombination to Open-Circuit Voltage in Sandwich-Type Thin-Film Solar Cells

Oskar J. Sandberg,* Anton Sundqvist, Mathias Nyman, and Ronald Österbacka
Department of Natural Sciences, Center for Functional Materials, Åbo Akademi University, Porthaninkatu 3, 20500 Turku, Finland
(Received 11 February 2016; published 12 April 2016)

To avoid surface recombination at the contacts and ensure efficient charge collection and high open-circuit voltages (V_{OC}) in organic bulk heterojunction and perovskite solar cells, selective contacts with optimized energy levels are needed. However, a detailed theoretical understanding of how the device performance is affected by surface recombination at the contacts is still lacking. In this work, the influence of surface recombination on the open-circuit voltage in sandwich-type solar cells, with optically thin active layers, is clarified using numerical simulations. Furthermore, analytical expressions are derived, directly relating V_{OC} to relevant device parameters, such as surface recombination velocity (S_p), mobility, and active layer thickness. At large S_p, the surface recombination is determined by diffusion-limited transport in the bulk. By reducing S_p, thus increasing the charge selectivity of the electrode, the surface recombination is eventually reduced as the transport becomes limited by interface kinetics at the contact. Depending on the interplay between surface recombination and bulk recombination, and the properties of the contacts, different operating regimes are identified featuring different light ideality factors and thickness dependences.

DOI: 10.1103/PhysRevApplied.5.044005

I. INTRODUCTION

Sandwich-type thin-film solar cells, such as organic or perovskite-based solar cells, hold great potential for future large-scale energy production [1–5]. Recently, in order to minimize energetic losses, a great deal of effort has been made trying to understand and maximize the open-circuit voltage (V_{OC}) [6–15]. V_{OC} corresponds to the voltage V when the total current under illumination is zero. At these conditions the total photogeneration rate is exactly balanced by recombination, where the recombination can either occur in the bulk or at the contacts as surface recombination. For a solar cell that ideally extracts holes at the anode and electrons at the cathode under operating conditions, the surface recombination is quantified by the rate of carriers that are extracted at the wrong electrode, i.e., electrons at the anode and holes at the cathode [10,16,17].

A quantity typically associated with the dominating recombination mechanism at open-circuit conditions, relating V_{OC} to the light intensity via [6,17–20]

$$qV_{OC} = mkT\ln(I_L) + \text{const}, \tag{1}$$

is the so-called light ideality factor m; here, I_L is a normalized light intensity, q is the elementary charge, T is the temperature, and k is the Boltzmann constant. In the case when surface recombination is negligible at open circuit, all photogenerated carriers recombine within the bulk. In this case, for a bulk recombination rate $R \propto (\sqrt{np})^{\alpha} \sim n^{\alpha}$ of recombination order α (for *free* carriers), where n and p is the free-carrier density for electrons and holes, respectively, a light ideality factor of $m = m_R$ is expected, where [19,20]

$$m_R = \frac{2}{\alpha}. \tag{2}$$

The largest V_{OC} is obtained when direct radiative recombination between free carriers ($\alpha = 2$) presents the only recombination pathway in the bulk [7,10,21]. However, trap-assisted recombination via exponentially distributed tail states ($1 < \alpha < 2$) and/or midgap states ($\alpha \sim 1$) is inevitably also present to some extent in most materials. When this type of recombination dominates m between 1 and 2 is typically expected [6,17,22,23].

In organic and perovskite-based solar cells, however, both V_{OC} and m have also been found to be strongly dependent on the choice of the electrode materials [17,24–26]. In this case, losses due to unoptimized energy levels at the electrodes can typically be traced back to an increased surface recombination at the contacts, typically manifested by an electrode work-function (WF) dependence of the open-circuit voltage [1,7,26–33]. The surface recombination has also been found to be dependent on both charge transport properties and the thickness of the active layer [7,10,16,34]. To reduce losses due to surface recombination, a charge-selective electrode interlayer is typically used at the contact. In the ideal case, this layer allows for only one carrier type to be extracted while the extraction of the other type is prevented. Indeed, an increase in V_{OC} is

*osandber@abo.fi

typically seen upon inserting a charge-selective buffer layer between the electrode and the active layer [25,35–38]. However, despite the vast progress made in the last decade, an analytic description of how surface recombination at the contacts influences the open-circuit voltage is still lacking.

In this paper, the influence of surface recombination on the open-circuit voltage in sandwich-type solar cells, with optically thin active layers, is investigated. Using a numerical device model, the effect of surface recombination velocity, mobility, photogeneration, and bulk recombination rate is simulated with different energy levels at the contacts. Furthermore, analytical expressions for V_{OC} are derived. Based on the results, different regimes can be identified, exhibiting different photogeneration dependences and light ideality factors. Because of the generality of our approach, the obtained results apply not only to organic and perovskite solar cells but to other sandwich-type thin-film solar cell technologies as well.

II. THEORETICAL BACKGROUND

The device to be investigated consists of an active layer, sandwiched between a hole-extracting anode ($x = 0$) and an electron-extracting cathode ($x = d$); the energy-level diagram is shown in Fig. 1. The active layer is treated as an effective semiconductor where the hole (electron) transport takes place at the valence (conduction) transport level E_v (E_c). The (effective) electrical band gap E_g is given by the difference between the respective transport levels. The charge transport is described by the continuity equation [21,39]

$$\underset{(-)}{+}\frac{1}{q}\frac{dJ_{p(n)}}{dx} = G - R, \tag{3}$$

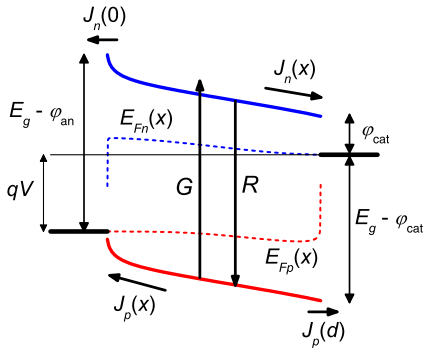

FIG. 1. The energy-level diagram of a sandwich-type thin-film solar cell. The transport levels E_v and E_c are indicated by the red and blue levels, respectively. The corresponding quasi-Fermi-levels E_{Fp} and E_{Fn} are given by the dashed lines. The photogenerated holes and electrons are to be extracted at the anode and the cathode, respectively. The corresponding energetic injection barriers are denoted by φ_{an} and φ_{cat}. The surface recombination at the anode ($x = 0$) and the cathode ($x = d$) is determined by $J_n(0)$ and $J_p(d)$, respectively.

where G is the photogeneration rate while the hole and electron current densities are, respectively, given by

$$J_p(x) = p\mu_p\frac{dE_{Fp}}{dx}, \tag{4}$$

$$J_n(x) = n\mu_n\frac{dE_{Fn}}{dx}, \tag{5}$$

where $\mu_{p(n)}$ is the hole (electron) mobility and $E_{Fp(n)}$ is the hole (electron) quasi-Fermi-level. The classical Einstein relation is assumed for carriers in the transport levels [39,40], implying that $p = N_v\exp[(E_v - E_{Fp})/kT]$ and $n = N_c\exp[(E_{Fn} - E_c)/kT]$, where $N_{v(c)}$ is the effective density of states for holes (electrons). N_v and N_c are to be considered effective quantities, incorporating the width of the transport levels (due to disorder, etc.) [27,41].

Integrating the continuity equation, the total current density $J = J_p(x) + J_n(x)$ can be expressed as

$$J = -q\int_0^d (G - R)dx + J_n(0) + J_p(d), \tag{6}$$

where d is the thickness of the active layer. The surface recombination, determined by the minority carrier current densities at the electrodes, is described as

$$J_p(d) = qS_p[p(d) - p_{cat}], \tag{7a}$$

$$J_n(0) = qS_n[n(0) - n_{an}], \tag{7b}$$

where $p_{cat} = N_v\exp\{-[(E_g - \varphi_{cat})/kT]\}$ is the equilibrium hole density at the cathode, $n_{an} = N_c\exp\{-[(E_g - \varphi_{an})/kT]\}$ is the equilibrium electron density at the anode, while S_p and S_n are the effective recombination velocities for holes at the cathode and electrons at the anode, respectively. Here the energy levels of the contacts enter via the injection barriers φ_{cat} for electrons at the cathode and φ_{an} for holes at the anode, determined by the respective energy-level offsets (see Fig. 1). Note that if recombination losses are negligible at short-circuit conditions then $J_{sc} = -qG_L d$, where $G_L \equiv (1/d)\int_0^d G(x)dx$ is the spatially averaged photogeneration rate.

The bulk recombination rate is given by

$$R = \beta_R(np - n_i^2), \tag{8}$$

where $n_i^2 = N_cN_v\exp(-E_g/kT)$ and β_R is the recombination coefficient. The effect of trap-assisted recombination can be taken into account by introducing a carrier-density-dependent β_R [18,39,42]. In homogeneous low-mobility materials the recombination between a mobile and an oppositely charged (either mobile or trapped) carrier is typically described by Langevin's theory [42,43]; the recombination coefficient between two mobile carriers reads

$$\beta_L = \frac{q}{\varepsilon\varepsilon_0}(\mu_n + \mu_p). \tag{9}$$

In a phase-separated blend structure, however, the effect of morphology leads to a reduced recombination relative to Langevin [20,43–45]. Furthermore, if the recombination occurs via intermediate charge transfer (CT) states [8,11], having a finite probability to dissociate back to free carriers, this will reduce the recombination even further [10,46]. Typically, $\beta_R = \zeta\beta_L$, where the reduction factor ζ ranges between 1 and 10^{-3} in organic solar cells [43,46,47], while in perovskite solar cells ζ on the order of 10^{-5} have been reported [48].

The surface recombination velocity S_p is given by $S_p = c_p N_{st}$, where c_p is a capture coefficient for holes at the cathode surface and N_{st} is the surface density of recombination centers [39]. For a nonselective contact, being able to efficiently capture and extract both types of carriers, we expect S_p to be large. Since surface recombination (at the contact) is the inverse process of thermionic emission, S_p can also be expressed as $S_p = (A^{**}T^2/qN_v)$, where A^{**} is the effective Richardson constant [39,49]. The upper value of the recombination velocity is on the order of 10^6 to 10^7 cm/s [16,39].

To avoid surface recombination of holes at the cathode, however, S_p needs to be as small as possible. This may be achieved by inserting an electron-selective interlayer, inhibiting holes from traversing the contact. In this sense, a reduced S_p is directly correlated with an increased selectivity of the contact. In the ideal scenario $S_p = 0$, here defined as a *perfectly* selective contact, no holes (only electrons) are allowed to be extracted at the cathode. For two perfectly selective contacts $[J_n(0) = J_p(d) = 0]$, the open-circuit condition $J = 0$ is reached when the average photogeneration rate is balanced by the average recombination rate in the bulk and V_{OC} is given by the well-known relation [6,23]

$$qV_{\mathrm{OC,max}} = E_g - kT\ln\left(\frac{\beta_R N_v N_c}{G_L}\right). \tag{10}$$

In reality, however, depending on processing and/or operating (ambient) conditions, impurity-induced recombination centers are always present to some extent at the contacts, effectively leading to nonzero surface recombination velocities S_p and S_n.

For a device that ideally extracts holes at the anode, but has a nonzero S_p at the cathode, the surface recombination current (at the cathode) can generally be expressed as

$$J_p(d) = \frac{qv_{d,p}p_{\mathrm{cat}}}{\left(1 + \frac{v_{d,p}}{S_p}\right)}\left[\exp\left(\frac{qV}{kT}\right) - 1\right], \tag{11}$$

for $J_p(d) \neq 0$, as shown in Appendix A, where

$$v_{d,p} \equiv \frac{\mu_p kT}{q}\left[\int_0^d \frac{J_p(x)}{J_p(d)} e^{[E_v(d) - E_v(x)]/kT} dx\right]^{-1} \tag{12}$$

is an effective hole diffusion velocity in the bulk, associated with transport of holes to the cathode interface. Considering Eq. (11) we see that the surface recombination at the cathode depends on both transport and contact properties, and is determined by a two-step process: (i) the diffusion of a hole to the cathode interface, and (ii) the recombination of the hole at the active layer-cathode interface. Depending on which process is limiting, the surface recombination is either limited by diffusion ($S_p \gg v_{d,p}$) or by the kinetics at the interface ($S_p \ll v_{d,p}$).

III. RESULTS AND DISCUSSION

In this section, the impact of surface recombination on the open-circuit voltage is investigated. In the general case, $v_{d,p}$ depends on both transport and recombination properties in the bulk, as well as the electric field. However, aided by numerical simulations, analytical approximations can be obtained, allowing for both $J_p(d)$ and V_{OC} to be evaluated. In the following, unless otherwise stated, an undoped active layer of thickness $d = 150$ nm with symmetric mobilities $\mu_p = \mu_n = 5 \times 10^{-3}$ cm^2 V^{-1} s^{-1} is assumed; the default parameters are given in Appendix B. The photogeneration rate of free carriers is taken to be spatially constant, $G = G_L$, and always large enough for $V_{\mathrm{OC}} \gg kT/q$ to be valid. The extraction of holes at the anode and electrons at the cathode is assumed to be ideal. Consequently, we have $n(d) = n_{\mathrm{cat}}$, where n_{cat} is the equilibrium electron density at the cathode. (For the case with a reduced extraction velocity for majority carriers, see Ref. [27] and references therein.)

A. The influence of surface recombination at Ohmic contacts

We first consider the case when both of the contacts are Ohmic, corresponding to electrodes with optimized energy levels. The cathode contact is said to be Ohmic for electrons, when the electron current is not limited by the cathode. This implies that (i) a considerable accumulation of free electrons (and energy-level bending) is present in the vicinity of the cathode and (ii) that $n_{\mathrm{cat}} \gg n_{\mathrm{ph}}$, where

$$n_{\mathrm{ph}} = \sqrt{np} = n_i \exp\left(\frac{qV_{\mathrm{ph}}}{2kT}\right), \tag{13}$$

and $qV_{\mathrm{ph}}(x) = E_{Fn} - E_{Fp}$. An analogous situation is valid for holes at the anode. JV curves for a solar cell with perfectly selective ($S_p = 0$) and nonselective ($S_p \to \infty$) contacts are simulated in Figs. 2(a) and 2(b), respectively, for varying $\beta_R = \zeta\beta_L$. For simplicity, $S_n = S_p$ is assumed. The corresponding V_{OC} as a function of surface recombination velocity is simulated in Fig. 2(c), as indicated by the solid lines. It is seen that at a small enough S_p ($S_p \to 0$), V_{OC} is essentially independent of S_p; in this regime V_{OC} follows Eq. (10), increasing with a decreasing β_R. When S_p

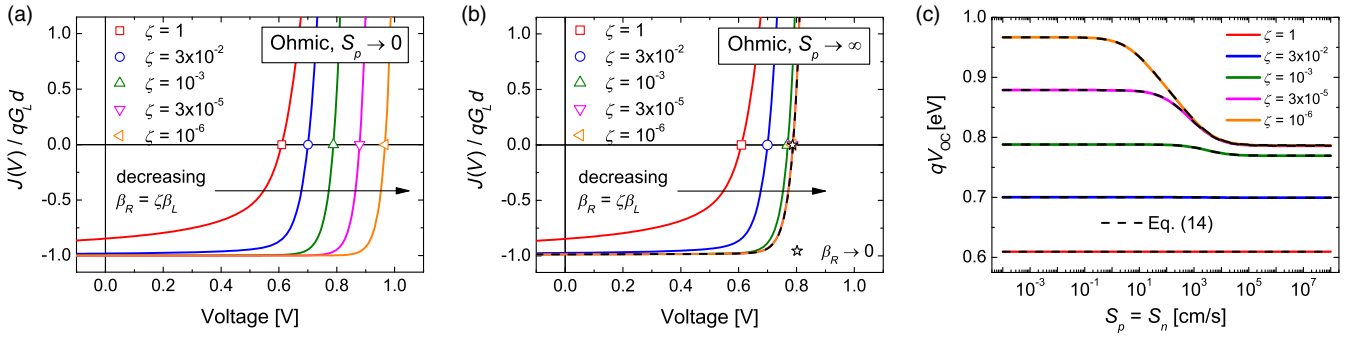

FIG. 2. Simulated JV curves and V_{OC} under 1 sun illumination for the case with Ohmic contacts at different $\beta_R = \zeta\beta_L$ and assuming $S_p = S_n$. In (a) and (b) JV curves for perfectly selective ($S_p \to 0$) and nonselective ($S_p \to \infty$) contacts are shown, respectively. The case with no bulk recombination, $\beta_R \to 0$, is indicated by the dashed line in (b) for comparison. In (c) the corresponding S_p dependence of V_{OC} (in units of eV) is simulated (solid lines). The analytical prediction Eq. (14) is indicated by the dashed lines.

is large, however, a saturation of V_{OC} (with a decreasing β_R) starts to appear at $\zeta < 10^{-3}$, as V_{OC} becomes independent of the magnitude of recombination in the bulk. As a result, for small β_R, a substantial loss due to surface recombination is inevitably present at large S_p.

To understand the reason for this behavior in more detail, typical energy-level diagrams at $V = V_{OC}$ for the two limiting regimes $S_p \to \infty$ and $S_p \to 0$ are simulated in Figs. 3(a) and 3(b), respectively. In the bulk the quasi-Fermi-levels are essentially constant throughout the active layer with the quasi-Fermi-level splitting qV_{ph}, on average, being equal to qV_{OC}. Concomitantly,

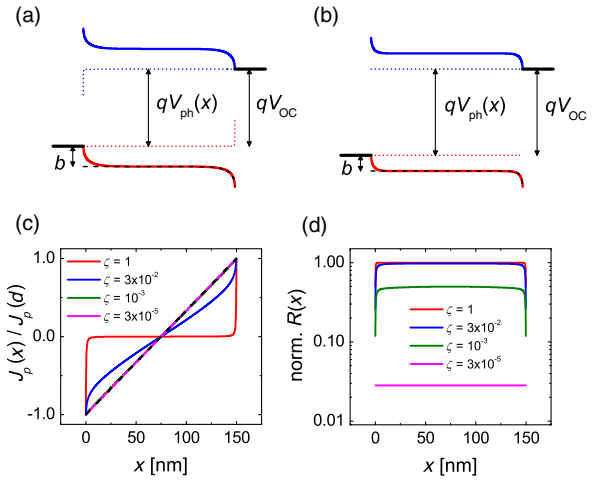

FIG. 3. Simulated energy-level diagrams at the open circuit of a device with Ohmic contacts and $S_p = S_n$ for (a) a large S_p and (b) $S_p \to 0$, corresponding to dominating surface and bulk recombination, respectively. Equation (15), as indicated by the dashed black line, has been included for comparison in (a) and (b). In (c) and (d) the corresponding normalized hole current densities $J_p(x)/J_p(d)$ and bulk recombination rates $R(x)/G_L$ are shown, respectively (at $V = V_{OC}$), for different $\beta_R = \zeta\beta_L$ in the limit of large $S_p = S_n$. The dashed line in (c) corresponds to the case with $\beta_R \to 0$.

$\int_0^d (G - R)dx \approx [G_L - \beta_R n_i^2 \exp(qV_{OC}/kT)]d$. Under open-circuit conditions, it then follows from Eqs. (6) and (11) that

$$qV_{OC} = E_g - kT \ln\left[\frac{(\beta_R + \beta_{S,p} + \beta_{S,n})N_v N_c}{G_L}\right], \quad (14)$$

where $\beta_{S,p} = (v_{d,p} p_{cat}/n_i^2 d)[1 + (v_{d,p}/S_p)]^{-1}$ is an effective capture coefficient for the surface recombination of holes at the cathode, $\beta_{S,n}$ is the respective coefficient for electrons at the anode; in our case $\beta_{S,n} = \beta_{S,p}$. While β_R is a material parameter, $\beta_{S,p}$ is dependent on device properties, taking surface effects into account. As a result, the open-circuit voltage is in general device dependent; only in the limit of perfectly selective contacts is V_{OC} given by Eq. (10).

1. Dominating surface recombination

When β_R is small (compared to $\beta_{S,p}$), surface recombination dominates at $V = V_{OC}$. With Ohmic contacts, an accumulation of injected carriers is present at both electrodes, giving rise to bending of the transport levels. Considering the transport of holes, the energy-level bending at the anode can be treated as an effective injection barrier b for *holes* at the anode [50]. Under these conditions, assuming that n, $p \to n_{ph}$ well within the active layer, the energy-level bending of $E_v(x)$ induced by the electron-Ohmic cathode is well approximated by [51]

$$E_v(x) \approx E_v(d) - 2kT \ln\left\{\frac{\coth\left[(1 + \frac{d-x}{L_{cat}})\sqrt{\frac{n_{ph}}{n_{cat}}}\right]}{\coth\left(\sqrt{\frac{n_{ph}}{n_{cat}}}\right)}\right\}, \quad (15)$$

where $L_{cat} = \sqrt{2\varepsilon\varepsilon_0 kT/q^2 n_{cat}}$. Taking $R = \beta_R n_{ph}^2$ to be constant throughout the active layer at $V = V_{OC}$, as implied by Fig. 3, the current density can be evaluated analytically as $J_p(x) = J_p(d)[(2x/d) - 1]$. In conjunction with

Eq. (15), we find $v_{d,p} \approx \mu_p kT/qL_{\mathrm{cat}}$ for $n_{\mathrm{ph}} \ll n_{\mathrm{cat}}$ (see Ref. [52]); hence, for Ohmic contacts

$$\beta_{S,p} = \frac{\mu_p kT}{qn_i^2 d} \frac{p_{\mathrm{cat}}/L_{\mathrm{cat}}}{(1+\frac{\mu_p kT}{qS_p L_{\mathrm{cat}}})}. \quad (16)$$

An analogous treatment is valid for surface recombination of electrons at the anode.

Now, upon comparing the analytical prediction Eq. (14) (dashed lines) with $\beta_{S,p}$ given by Eq. (16) and the simulated V_{OC} (solid lines) in Fig. 2(c), an excellent agreement over the entire range of S_p is found. It can be seen that also the photogeneration rate and mobility dependence of V_{OC} as simulated in Figs. 4(a) and 4(b) (solid lines), respectively, for different β_R and S_p, is well reproduced by Eq. (14) (dashed lines). The effect of surface recombination on the open-circuit voltage can now be explained in detail. By reducing the bulk recombination rate, the recombination at the surface eventually becomes comparable to the one in the bulk, and as $\beta_R \ll \beta_{S,p}$, the photogeneration is completely canceled by surface recombination at open-circuit conditions. In this limit, $qV_{\mathrm{OC}} = E_g - kT\ln(2\beta_{S,p}N_v N_c/G_L)$, explaining the saturation of V_{OC} with decreasing ζ. Note the similarity between this type of surface recombination and direct bimolecular bulk recombination.

At large S_p, i.e., when $S_p \gg v_{d,p}$, the surface recombination is diffusion limited and the V_{OC} is essentially independent of S_p. Under these conditions, the effective capture coefficient $\beta_{S,p}$ is directly proportional to the mobility (behaving similar to a reduced β_L) but inversely proportional to the active layer thickness; hence, $qV_{\mathrm{OC}} \propto -kT\ln(\mu_p/d)$. As a result, V_{OC} decreases with an increasing mobility and a decreasing thickness, in agreement with previous findings by Kirchartz *et al.* and Tress *et al.* [10,16]. When $S_p \ll v_{d,p}$, on the other hand, the surface recombination becomes limited by the interface kinetics at the electrode. In this case, an S_p-dependent V_{OC} regime, $qV_{\mathrm{OC}} \propto -kT\ln(S_p/d)$, is entered [as $\beta_{S,p} \propto (S_p/d)$]; by decreasing S_p, the magnitude of surface recombination is reduced and V_{OC} increased. We note that the d dependence of V_{OC}, that is present regardless of whether the surface recombination is limited by diffusion or kinetics at the electrode interface, originates from the photocurrent, $J_{\mathrm{ph}} = q\int_0^d G(x)dx = qG_L d$, that needs to be compensated for to reach the open-circuit condition. Since the diffusion process is limited by holes diffusing against the energy-level bending at the cathode, the diffusion-limited transport $(v_{p,d})$ *per se* does not depend on d in this case (*Ohmic* contacts).

2. Dominating bulk recombination

When $\beta_{S,p}$ and β_R are of the same order of magnitude, $\beta_{S,p}$ is still well approximated by Eq. (16). As $S_p \to 0$, the limit $\beta_R \gg \beta_{S,p}$ is eventually reached. In this case, losses due to surface recombination are negligible relative to the recombination in the bulk, and V_{OC} approaches $V_{\mathrm{OC,max}}$ [Eq. (14) becomes identical to Eq. (10)]. When S_p is large, on the other hand, $\beta_{S,p}$ starts to deviate from Eq. (16) as $\beta_R \gg \beta_{S,p}$, in accordance with Fig. 3(c); at $\zeta = 1$ Eq. (16) underestimates $\beta_{S,p}$ by a factor of 2. However, since this occurs when $\beta_R \gg \beta_{S,p}$, the error made in Eq. (16) is completely overshadowed by the large bulk recombination as V_{OC} becomes independent of $\beta_{S,p}$.

A necessary condition to obtain the optimum V_{OC} given by Eq. (10) is that $\beta_{S,p} \ll \beta_R$, corresponding to $S_p \ll \beta_R n_i^2 d/p_{\mathrm{cat}}$. Consequently, at lower β_R, a smaller S_p is required. Note that, depending on the device parameters, for Ohmic contacts β_S/β_L between $\sim 10^{-2}$ and 10^{-4} are expected at large S_p. This clearly demonstrates the importance of the contacts, especially in solar-cell materials exhibiting long recombination lifetimes and/or relatively high mobilities. Unless the charge selectivity at the contacts can be ensured, the V_{OC} becomes limited by surface recombination rather than by bulk recombination.

B. The influence of surface recombination at non-Ohmic contacts

Under conditions when the energy levels at the cathode are mismatched a non-Ohmic contact may be formed. This occurs when the injection barrier φ_{cat} is large enough for $n_{\mathrm{cat}} \ll n_{\mathrm{ph}}$, where $n_{\mathrm{cat}} = N_c e^{-(\varphi_{\mathrm{cat}}/kT)}$, corresponding to the

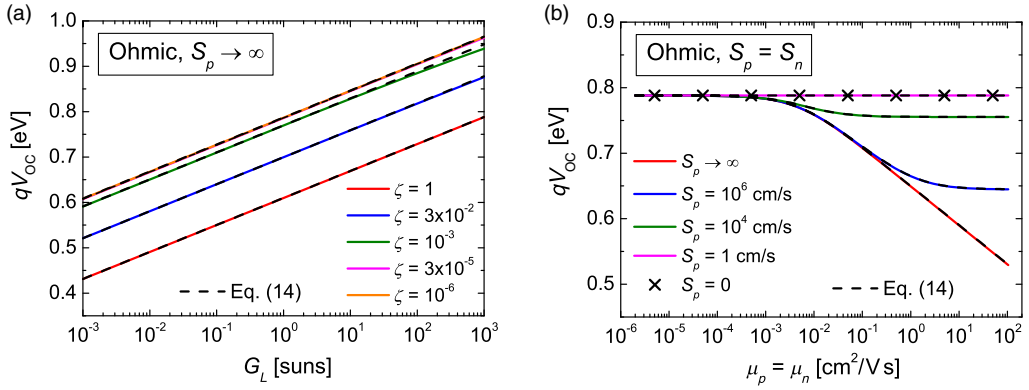

FIG. 4. Simulated V_{OC} for a device with Ohmic contacts and $S_n = S_p$. In (a) the photogeneration dependence with a varying degree of bulk recombination $\beta_R = \zeta\beta_L$. In (b) The mobility dependence (at 1 sun) for different S_p, assuming a fixed $\beta_R = 5.17\times 10^{-12}$ cm^3 s^{-1}. The analytical prediction Eq. (14) is indicated by the dashed lines.

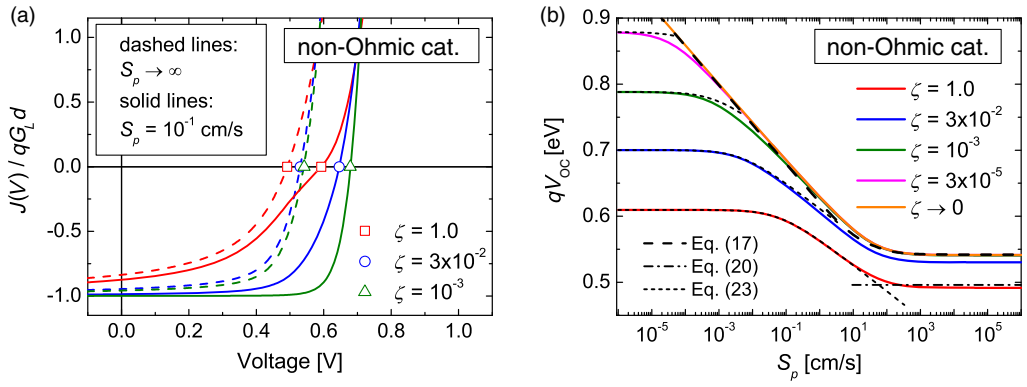

FIG. 5. Simulated JV curves and V_{OC} of a device (under illumination) with a non-Ohmic contact at the cathode ($\varphi_{cat} = 0.4$ eV) are depicted in (a) and (b), respectively, for varying $\beta_R = \zeta\beta_L$ and surface recombination velocity S_p [solid lines in (b)]. The anode is assumed to be perfectly selective [$J_n(0) = 0$] and Ohmic for holes.

case with an increased (or too high) WF at the cathode contact. It is a fairly well-known phenomenon that the WFs of both low-WF metals and metal-oxide-based (inter) electrode layers (e.g., ITO, TiO_2, ZnO, NiO_x) are prone to degradation, depending on processing, ambient, and/or operating conditions [30,33,53–55], and might thus result in non-Ohmic contacts. In the case of two non-Ohmic *nonselective* contacts, V_{OC} is limited by the work-function difference between the contacts, $qV_{OC} = E_g - \varphi_{cat} - \varphi_{an}$ [26–29]. On the other hand, in the limit of two *perfectly* selective contacts it has been shown that $V_{OC} \to V_{OC,max}$, independent of the energy levels at the electrodes [10,21]; see Eq. (10). In the remainder of this section, the influence of surface recombination of holes at a non-Ohmic cathode is investigated for a general surface recombination velocity S_p. To avoid interference from the surface recombination of electrons, the anode is taken to be perfectly selective [$J_n(0) = 0$] and Ohmic for holes. At the non-Ohmic cathode, we assume $\varphi_{cat} = 0.4$ eV.

The JV curves and the S_p dependence of V_{OC} for a device under illumination is simulated in Figs. 5(a) and 5(b), respectively, with different $\beta_R = \zeta\beta_L$. As expected, when $S_p \to 0$, the V_{OC} are identical to the case with Ohmic contacts (Fig. 2). At large and moderate S_p, however, the V_{OC} in Fig. 5(b) are markedly lower, always well below $V_{OC,max}$, even at large β_R. Furthermore, the smaller β_R is, the more prominent the loss due to surface recombination becomes. The effect of increasing the injection barrier is to increase the magnitude of surface recombination current $J_p(d)$ at the cathode, growing exponentially with φ_{cat} (via p_{cat}). Consequently, due to the non-Ohmic contact, the surface recombination is considerably larger in this case. In the limiting case when surface recombination at the cathode is dominating, we expect

$$qV_{OC} = E_g - \varphi_{cat} - kT \ln\left[\frac{v_{d,p}N_v}{G_L d}\left(1 + \frac{v_{d,p}}{S_p}\right)^{-1}\right]. \quad (17)$$

Under these conditions, Eq. (3) reveals $J_p(x) \approx qG_L x = J_p(d)[x/d]$. Approximating $E_v(x) = E_v(d) - qF[d - x]$, we obtain

$$v_{d,p} = \frac{\mu_p F}{\frac{kT}{qFd}(e^{qFd/kT} - 1) - 1}, \quad (18)$$

where F is the electric field at $V = V_{OC}$ given by

$$F \approx \min\left(\frac{V_{OC} - V_{bi}^*}{d}, 0\right). \quad (19)$$

Here, $V_{bi}^* = (E_g - \varphi_{cat} - b)/q$ is the effective built-in voltage, taking the energy-level bending at the anode into account via b. For $F < 0$, we assume $b = 0.24$ eV at $d = 150$ nm. The corresponding energy-level diagrams at $V = V_{OC}$ are simulated in Fig. 6.

In deriving Eqs. (17) and (18) we assumed that (i) the bulk recombination is negligible compared to surface recombination so that $J_p(d) = qG_L d$ [$R \approx 0$ in Eq. (3)],

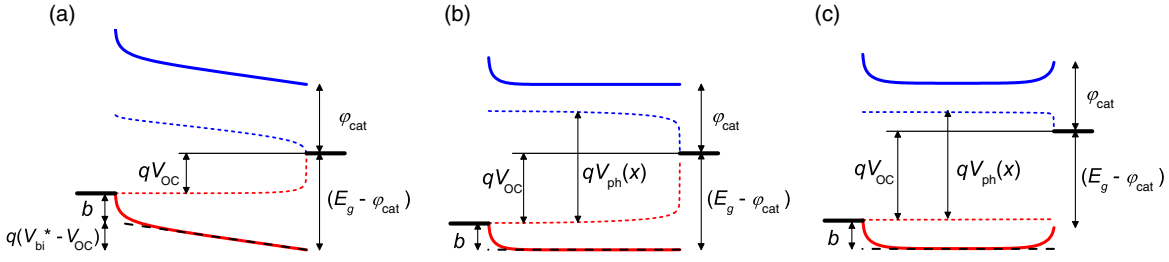

FIG. 6. Simulated energy-level diagrams at $V = V_{OC}$ for a device with a non-Ohmic contact at the cathode and negligible recombination in the bulk ($\beta_R \to 0$). The case with $S_p \gg v_{d,p}$ is depicted in (a) and (b) in the limit of low and high light intensities, respectively. The case with $S_p \ll v_{d,p}$ is shown in (c). The anode is assumed to be perfectly selective and Ohmic for holes. The approximation $E_v(x) = E_v(d) - qF[d - x]$, with F given by Eq. (19), is indicated by the dashed lines.

and (ii) that the electric field at open-circuit conditions is constant, $F \leq 0$. For a general S_p and β_R, however, neither of these assumptions needs to be true. In the following, the two limiting cases $S_p \gg v_{d,p}$ and $S_p \ll v_{d,p}$ are analyzed in more detail and the impact of a nonzero bulk recombination clarified.

1. Diffusion-limited surface recombination

For $S_p \gg v_{d,p}$, V_{OC} is independent of S_p and determined by diffusion-limited transport and recombination in the bulk. In this limit, Eq. (17) simplifies as $qV_{\mathrm{OC}} = E_g - \varphi_{\mathrm{cat}} - kT\ln(v_{d,p}N_v/G_L d)$, with $v_{d,p}$ given by Eq. (18). In case of negligible bulk recombination, we thus expect $qV_{\mathrm{OC}} \propto -kT\ln(\mu_p/d^2)$, implying a stronger thickness dependence compared to the case with Ohmic contacts. In Figs. 7(a) and 7(b) the light-intensity dependence and mobility dependence of V_{OC} is simulated, respectively. Indeed, under conditions when the bulk recombination is negligible compared to surface recombination, corresponding to small β_R and large μ_p, the simulated V_{OC} in Fig. 7 are well reproduced by Eq. (17). At low light intensities ($V_{\mathrm{bi}}^* - V_{\mathrm{OC}} \gg kT/q$), the open circuit is reached when the total photogeneration is canceled by the surface recombination of holes, diffusing from the Ohmic anode towards the cathode against a roughly constant electric field [see Fig. 6(a)]. In this case, V_{OC} is dependent on the electric field and increases with the decreasing magnitude of F, as $v_{d,p} \approx \mu_p|F|$. At higher intensities and/or larger d, Eq. (18) approaches $v_{d,p} \to 2\mu_p kT/qd$, as the bulk becomes dominated by photogenerated carriers that efficiently screen the electric field within the active layer [see Fig. 6(b)], resulting in a purely diffusion-driven surface recombination at the cathode.

While the V_{OC} in Fig. 7(a) is accurately described by Eq. (17) in the regime of negligible bulk recombination ($R \approx 0$), at high enough light intensities and/or large β_R a deviation from Eq. (17) is eventually obtained as the bulk recombination becomes significant. Typical energy-level diagrams at V_{OC} in this β_R-dependent regime are simulated in Fig. 10(a). Well within the active layer, the carrier density is limited by bulk recombination and $V_{\mathrm{ph}} = V_{\mathrm{OC,max}}$; the loss in photovoltage, $\Delta E_{Fn} = q(V_{\mathrm{OC,max}} - V_{\mathrm{OC}})$, mainly takes place in a region close to the cathode where surface recombination is dominating.

This behavior can be understood in terms of an effective diffusion length L_n^*, corresponding to the equivalent average distance a carrier travels before it recombines in the bulk. If we effectively assume that all carriers photogenerated within the distance $L_n^* \ll d$ from the cathode interface are extracted, while the rest recombine in the bulk: $J_p(x) \approx qG_L(x - d + L_n^*)$ when $x \in [d - L_n^*, d]$, and $J_p(x) \approx 0$ otherwise. Under these circumstances, an approximation can be obtained when V_{OC} is close to flatband conditions, we obtain [56]

$$qV_{\mathrm{OC}} \approx E_g - \varphi_{\mathrm{cat}} - kT\ln\left(\frac{v_{d,p}^* N_v}{G_L L_n^*}\right), \tag{20}$$

with $v_{d,p}^* = (2\mu_p kT/qL_n^*)[1 - (qFL_n^*/3kT)]$, where (see Appendix A)

$$L_n^* \approx \left(\frac{\mu_{\mathrm{eff}} kT}{q\sqrt{\beta_R G_L}}\right)^{1/2}, \tag{21}$$

and $\mu_{\mathrm{eff}} = 2\sqrt{\mu_p \mu_n}$. Note that $F \leq 0$.

Comparing with the simulated V_{OC} in Fig. 7 a good agreement with Eq. (20) is obtained at high enough intensities, when the open-circuit voltage is close to flatband conditions; in the limit $F \to 0$,

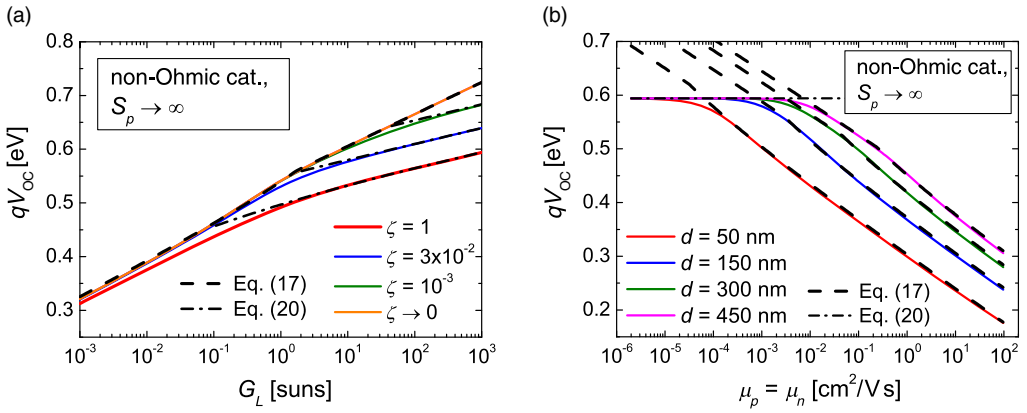

FIG. 7. Simulated V_{OC} (solid lines) for a device having a non-Ohmic contact at the cathode in the limit of large S_p. In (a) the photogeneration dependence of V_{OC} is shown for varying $\beta_R = \zeta\beta_L$ (at $d = 150$ nm). In (b) the corresponding mobility dependence of V_{OC} (at 1 sun) for different layer thickness d, assuming a fixed $\beta_R = 5.17 \times 10^{-12}$ cm^2/V s. Equations (17) and (20) are indicated by dashed and dash-dotted lines, respectively. In Eq. (17) (for $F < 0$) we assume a value of $b = 0.24$ eV at $d = 150$ nm and that $b \propto kT\ln(d^2)$ [50].

$$qV_{\mathrm{OC}} \to E_g - \varphi_{\mathrm{cat}} - \frac{kT}{2}\ln\left(\frac{\mu_p \beta_R N_v^2}{\mu_n G_L}\right).$$

The effect of increasing β_R and/or light intensity is to reduce L_n^* as the probability for carriers to recombine inside the bulk increases. On average, only holes within the distance L_n^* from the cathode are able to reach the contact. Concomitantly, the surface recombination becomes restricted to this spatial region, and V_{OC} becomes independent of d. Conversely, by increasing the mobility or reducing the layer thickness so that $d < L_n^*$, holes are more probable to be extracted at the cathode than to recombine in the bulk, and the regime of negligible bulk recombination [Eq. (17)], where the surface recombination dominates over the entire layer, is entered. The crossover between these two regimes occurs when $L_n^* \sim d$.

2. Interface kinetic-limited surface recombination

We next consider the case $S_p \ll v_{d,p}$, when the surface recombination is limited by the kinetics at the cathode interface. In this limit, V_{OC} is independent of $v_{d,p}$ and Eq. (17) approaches $qV_{\mathrm{OC}} = kT\ln(G_L d/S_p p_{\mathrm{cat}})$. The simulated generation dependence of V_{OC} with different $\beta_R = \zeta\beta_L$ is shown in Fig. 9(a) for $S_p = 10^{-1}$ cm/s. In Fig. 9(b), the mobility dependence of V_{OC} is simulated for varying S_p. As long as the surface recombination dominates, corresponding to the case when β_R is small and/or μ_p is large but V_{OC} is well below $V_{\mathrm{OC,max}}$, the V_{OC} is to a fair approximation given by Eq. (17). From the corresponding energy-level diagrams in Fig. 6(c), we see that a bias-induced upward-energy-level bending is present at the non-Ohmic cathode in this case. Since this energy-level bending was neglected in Eq. (18), leading to a severe overestimation of $v_{d,p}$, Eq. (17) underestimates the V_{OC} when $v_{d,p} \sim S_p$ (at high G_L). The energy-level bending is a direct consequence of the interface kinetic-limited hole transport, increasing the hole density at the cathode with increasing V_{OC}. Provided that $S_p \ll v_{d,p}$, we have [57]

$$p(d) = p_{\mathrm{cat}}\exp\left(\frac{qV_{\mathrm{OC}}}{kT}\right). \tag{22}$$

Furthermore, since the hole transport is not limited by the bulk, the hole quasi-Fermi-level is flat throughout the active layer in this limit.

At smaller S_p (or higher intensities) the bulk recombination eventually starts to dominate within the active layer. The corresponding energy-level diagrams at $V = V_{\mathrm{OC}}$ is shown in Fig. 8(b). Well within the active layer, bulk recombination is dominating ($R \approx G_L$) and the quasi-Fermi-level splitting is limited by $V_{\mathrm{ph}} = V_{\mathrm{OC,max}}$. In conjunction with the buildup of bias-induced holes at small S_p, this results in an excess of holes in the device ($p \gg n$), accumulating at the cathode interface in accordance with Eq. (22). Concomitantly, the bulk recombination close to the cathode cannot be neglected in this case; in the vicinity of the cathode we have $R(d) = \beta_R n_{\mathrm{cat}} p(d)$. However, as long as $J_p(d) \neq 0$, the bulk recombination rate close to the cathode will remain lower than the bulk recombination rate inside the active layer.

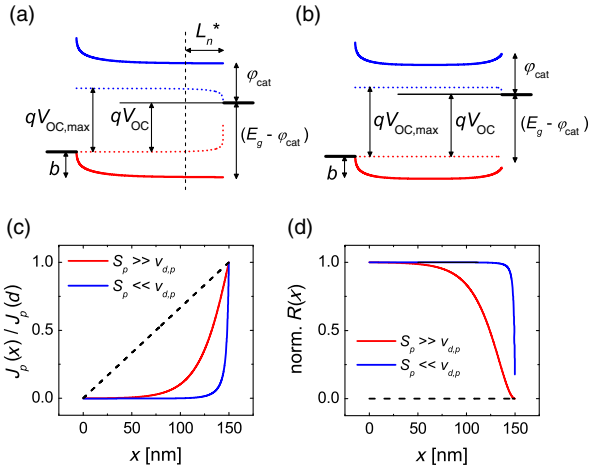

FIG. 8. Typical energy-level diagrams at $V = V_{\mathrm{OC}}$ for a device having a non-Ohmic contact at the cathode in the case when bulk recombination dominates well within the active layer. In (a) and (b) the cases $S_p \gg v_{p,d}$ and $S_p \ll v_{p,d}$ are simulated, respectively. In (c) and (d) the corresponding profiles for the normalized hole current densities $J_p(x)/J_p(d)$ and bulk recombination rates $R(x)/G_L$ are shown, respectively; the dashed lines corresponds to the case when $\beta_R \to 0$.

To satisfy the open-circuit condition $J_n(d) = -J_p(d)$, the photogenerated electrons, driven by the quasi-Fermi-level difference $\Delta E_{Fn} = q(V_{\mathrm{OC,max}} - V_{\mathrm{OC}})$, have to diffuse "uphill" over the upward energy level bending (induced by the holes) in order to be extracted at the cathode. Subject to these conditions, taking into account the decrease in R from $R \approx G_L$ to $R(d) = \beta_R n_{\mathrm{cat}} p(d)$ that a nonzero electron current (close to the cathode) brings about, we find

$$qV_{\mathrm{OC}} = E_g - kT\ln\left[\frac{(\beta_R + \frac{S_p}{n_{\mathrm{cat}} d_{\mathrm{eff}}})N_c N_v}{G_L}\right], \tag{23}$$

where $d_{\mathrm{eff}} = L_n^{**}$ when $L_n^{**} \ll d$, and $d_{\mathrm{eff}} \approx d$ when $L_n^{**} \gg d$, as shown in Appendix A. Here, $L_n^{**} = K^{-1}/\sqrt{p(d)}$ is a reduced effective diffusion length, with

$$K \approx \frac{\beta_R}{\mu_n}\sqrt{\frac{8\varepsilon\varepsilon_0}{kT}}\left[\sqrt{1 + \frac{8\varepsilon\varepsilon_0\beta_R}{q\mu_n}} + 1\right]^{-1} \tag{24}$$

being a parameter independent of S_p, but dependent on material properties of the active layer. In the following, we approximate $d_{\mathrm{eff}} \approx \min(L_n^{**}, d)$.

A striking agreement between Eq. (23) and the simulated V_{OC} in Fig. 9(a) is found at large enough β_R and/or high intensities, when the bulk recombination eventually starts

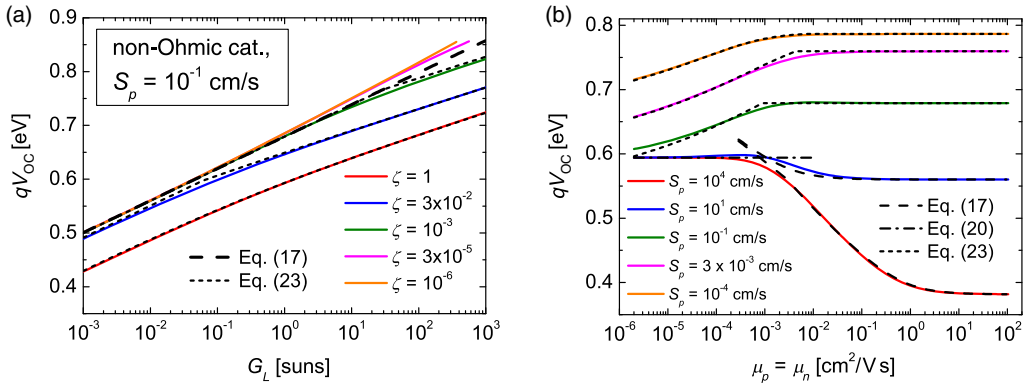

FIG. 9. Simulated V_{OC} (solid lines) of a device with a non-Ohmic cathode. In (a) the photogeneration dependence is depicted for different $\beta_R = \zeta\beta_L$ at $S_p = 10^{-1}$ cm/s. In (b) the corresponding mobility dependence of V_{OC} is shown for different S_p at 1 sun, assuming a fixed $\beta_R = 5.17 \times 10^{-12}$ cm^2/V s.

to compete with surface recombination. Also, the behavior at small S_p in Fig. 9(b) is well reproduced by Eq. (23). Note, however, that a deviation occurs when $L_n^{**} \sim d$. For $L_n^{**} \ll d$, Eq. (23) simplifies as

$$qV_{OC} \approx E_g - \varphi_{cat} - \frac{2kT}{3}\ln\left(K\frac{S_p N_v^{3/2}}{G_L}\right),$$

when $V_{OC} < V_{OC,max}$ (i.e., $S_p > \beta_R n_{cat} L_n^{**}$). The effect of reducing S_p is to reduce $J_p(d)$, simultaneously reducing the amount of electrons diffusing out at the cathode (as the upward energy-level bending becomes higher), leading to an increase in the V_{OC}. Interestingly, the V_{OC} increases with increasing μ_n/β_R in this case. This is due to the increased electron diffusion that needs to be compensated by a larger V_{OC} (smaller ΔE_{Fn}). As $S_p \to 0$, Eq. (23) eventually saturates and becomes identical to Eq. (10) ($V_{OC} \to V_{OC,max}$). Under these conditions, corresponding to negligibly small surface recombination, the driving force for electron extraction at the cathode vanishes ($\Delta E_{Fn} \to 0$) and essentially all recombination occurs in the bulk. The crossover from Eq. (23) to Eq. (10) occurs when $S_p < \beta_R n_{cat} d_{eff}$. Hence, for larger φ_{cat} (smaller n_{cat}) and/or small β_R, a smaller S_p is required to minimize losses due to surface recombination and ensure sufficient selectivity at the contact.

C. The light ideality factor

For the cases studied above, depending on the interplay between bulk and surface recombination and whether both of the contacts are Ohmic or not, distinctly different behaviors for the V_{OC} are expected. With $G_L \propto I_L$, the transition between a bulk recombination-dominated and a surface recombination-dominated regime is manifested as a generation dependence in the light ideality factor m in Eq. (1); in this case m is obtained from

$$m = \frac{q}{kT}\frac{\partial V_{OC}}{\partial[\ln(G_L)]}. \quad (25)$$

The change in the light ideality factor m may thereby be used to distinguish between surface recombination and bulk recombination at open-circuit conditions.

Consider first the case with Ohmic contacts. In this case V_{OC} is given by Eq. (14). Depending on the dominating recombination mechanism, we expect m to be close to $m = m_R$ when bulk recombination dominates ($\beta_R \gg \beta_S$) [58], while $m = 1$ when surface recombination dominates ($\beta_R \ll \beta_S$), in accordance with Eq. (25). Since $m_R = 1$ for direct bimolecular bulk recombination ($\alpha = 2$), $m = 1$ is also expected when this type of bulk recombination dominates, making it difficult to distinguish between direct bulk recombination and surface recombination in this case. Note, however, that a (different) thickness dependence in the V_{OC} is expected when surface recombination is dominating, provided that G_L is held the same (or normalized via $J_{ph} = qG_L d$).

In the case of trap-assisted bulk recombination via deep midgap states, a behavior similar to monomolecular recombination ($\alpha \sim 1$) is typically obtained, suggesting that $m_R = 2$. The impact of surface recombination on the light ideality factor, for trap-assisted bulk recombination and nonselective Ohmic contacts, is simulated in Fig. 10(a) (with negligible direct recombination). As expected, when bulk recombination dominates $m \approx 2$. However, at higher intensities and/or decreasing magnitude of bulk recombination, $m \to 1$ as surface recombination grows stronger, and in the limit when surface recombination dominates $m = 1$, in accordance with Eq. (14). Hence, neglecting the influence of surface recombination leads to an underestimation of m_R (and an overestimation of α) in this case. We note that similar transitions from $m = 1$ to $m = 2$ have been observed experimentally in the past, typically attributed to increased direct bulk recombination at high intensities. As demonstrated in Fig. 10(a), however, a similar behavior can also be caused by surface recombination.

Consider next the case when one of the contacts is non-Ohmic and nonselective ($S_p \gg v_{d,p}$). In Fig. 10(b) the light ideality factor in the case of a non-Ohmic contact at the cathode is simulated, assuming direct bulk recombination. The anode is assumed to be selective and Ohmic. Because of the high injection barrier, a substantial surface recombination is always present at the cathode, leading to a deviation from $m = m_R$. In the case when the bulk recombination is negligibly small compared to diffusion,

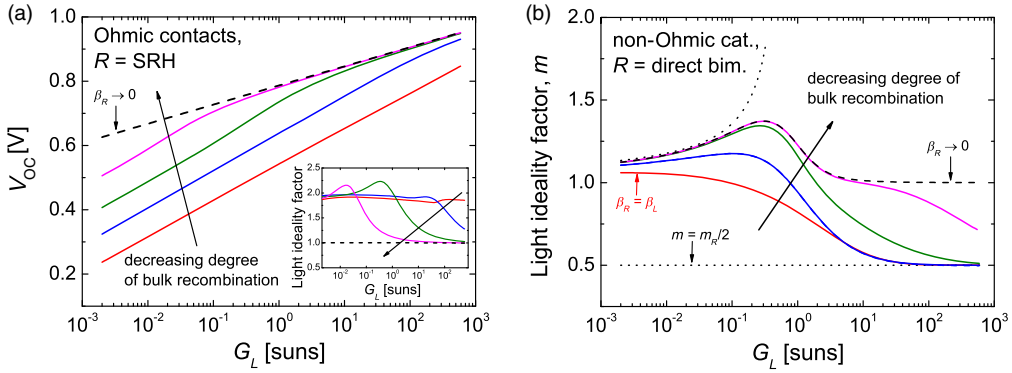

FIG. 10. The impact of surface recombination on the light ideality factor m. In (a) simulated photogeneration dependence of the open-circuit voltage V_{OC} for a device with Ohmic, but nonselective, contacts for varying degree recombination, assuming the recombination to be trap-assisted Shockley-Read-Hall (SRH) recombination only. The inset shows the corresponding light ideality factors. In (b) the light ideality factors for the case with a nonselective non-Ohmic cathode and direct bulk recombination is shown; the anode is Ohmic and perfectly selective. The two dotted lines in (b) correspond to $m = 1 + [kT/q(V_{bi}^* - V_{OC})]$ and $m = 1/2$.

V_{OC} is given by Eq. (17). At low light intensities, V_{OC} is dependent on the electric field, resulting in a light ideality factor $m \sim 1 + [kT/q(V_{bi}^* - V_{OC})] > 1$ that increases with increasing G_L. As flatband conditions are approached at higher light intensities (V_{OC} approaches V_{bi}^*), however, m peaks at a maximum value of $m \sim 1.4$ in Fig. 10(b), after which it decreases and plateaus to $m = 1$ (at high G_L). It can thus be seen that a light ideality factor well above $m = 1$ can also be caused by diffusion-limited surface recombination alone. Upon increasing β_R the recombination in the bulk eventually starts to limit the transport within the active layer, with V_{OC} well approximated by Eq. (20). In this case, a lower m is obtained and at high enough G_L we see that $m \to 1/2$, in accordance with Eq. (20). Note that for a more general recombination order of α (for free carriers), we instead expect a light ideality factor of $m \to m_R/2$ under these conditions [58]. This halving of $m = m_R$ (into $m = m_R/2$), expected upon changing the Ohmic cathode to a non-Ohmic one, is in good agreement with experimental data reported in the literature [28,59]. It should be noted that when both contacts are allowed to be nonselective, an additional reduction of m due to surface recombination at anode is present at high G_L and eventually as $qV_{OC} \to E_g - \varphi_{cat} - \varphi_{an}$, $m \to 0$.

On the other hand, by reducing S_p to such an extent that $S_p \ll v_{d,p}$, thus increasing the selectivity at the non-Ohmic cathode, the surface recombination at the cathode is reduced and becomes limited by the interface kinetics. Assuming a carrier-independent S_p, the V_{OC} is closely approximated by Eq. (23). If the recombination in the bulk remains negligible ($d_{eff} = d$), we expect $m = 1$. On the other hand, at higher G_L and larger β_R, when bulk recombination dominates within the active layer ($L_n^{**} \ll d$), a distinct ideality factor of $m = 2/3$ is expected when $V_{OC} < V_{OC,max}$. The appearance of $m = 2/3$ is in excellent agreement with the experimental light ideality factor obtained on inverted TiO_2-P3HT:PCBM solar cells, having unoptimized energy levels at the hole-blocking TiO_2-P3HT:PCBM interface [55].

IV. SUMMARY AND CONCLUSIONS

The impact of surface recombination on the open-circuit voltage in sandwich-type solar cells with optically thin layers has been clarified. Aided by numerical drift-diffusion simulations, we have investigated the influence of surface recombination velocity S_p at different magnitudes of the bulk recombination rates and energy levels at the contacts. At large S_p, the surface recombination is independent of S_p, and determined by diffusion-limited transport in the bulk and depends on the mobility μ_p. At small S_p, however, the surface recombination becomes limited by the interface kinetics at the contact, and reduces with decreasing S_p. Furthermore, analytical expressions have been derived, directly relating the open-circuit voltage to relevant charge transport, recombination, and contact properties, allowing for an analytic description of the underlying device physics. The analytical expressions are validated by numerical simulations, showing an excellent overall agreement over a wide range of surface recombination velocities, mobilities, and photogeneration rates. Depending on the interplay between surface recombination and bulk recombination different operating regimes can be identified, exhibiting different light ideality factors and thickness dependences.

ACKNOWLEDGMENTS

Partial financial support from the Magnus Ehrnrooth Foundation and from the Academy of Finland through Project No. 279055 is acknowledged. O. J. S. acknowledges funding from the National Graduate School of Nanoscience (NGS-nano) and M. N. acknowledges funding from The Society of Swedish Literature in Finland.

APPENDIX A: ANALYTICAL DERIVATIONS

1. The current density at the electrodes

Making use of $p = N_v e^{(E_v - E_{Fp})/kT}$, the hole current density equation [Eq. (4)] may be rearranged and integrated as

$$\int_0^d \frac{J_p(x)}{N_v \mu_p kT} e^{[E_v(d)-E_v(x)]/kT} dx = e^{[E_v(d)-E_{Fp}(0)]/kT} - e^{[E_v(d)-E_{Fp}(d)]/kT} = \frac{p_{\rm cat}}{N_v} e^{qV/kT} - \frac{p(d)}{N_v}, \quad \text{(A1)}$$

where $E_{Fp}(0) = E_F|_{\rm an}$, $E_g - \varphi_{\rm cat} = E_v(d) - E_F|_{\rm cat}$, and $qV = E_F|_{\rm cat} - E_F|_{\rm an}$ were used in the last step. Then, solving Eq. (A1) for $J_p(d)$, noting that $p(d) = [J_p(d)/qS_p] + p_{\rm cat}$, it follows that

$$J_p(d) = \frac{q v_{d,p} p_{\rm cat}}{(1 + \frac{v_{d,p}}{S_p})} (e^{qV/kT} - 1), \quad \text{(A2)}$$

where $v_{d,p} \equiv (\mu_p kT/q)\{\int_0^d [J_p(x)/J_p(d)] e^{[E_v(d)-E_v(x)]/kT} \times dx\}^{-1}$. An analogous treatment for electrons yields

$$\int_0^d \frac{J_n(x)}{N_c \mu_n kT} e^{[E_c(x)-E_c(0)]/kT} dx = e^{[E_{Fn}(d)-E_c(0)]/kT} - e^{[E_{Fn}(0)-E_c(0)]/kT} = \frac{n_{\rm an}}{N_c} e^{qV/kT} - \frac{n(0)}{N_c}, \quad \text{(A3)}$$

and

$$J_n(0) = \frac{q v_{d,n} n_{\rm an}}{(1 + \frac{v_{d,n}}{S_n})} (e^{qV/kT} - 1), \quad \text{(A4)}$$

where $v_{d,n} \equiv (\mu_n kT/q)\{\int_0^d [J_n(x)/J_n(0)] e^{[E_c(x)-E_c(0)]/kT} \times dx\}^{-1}$.

2. Analytical approximations of the effective diffusion length

At open-circuit conditions, the surface recombination current $J_p(d)$ is balanced by an equal but opposite electron current at the cathode; this electron current, driven by the gradient in E_{Fn}, can be expressed as

$$J_n(d) = -\frac{\mu_n kT n_{\rm cat}}{[\int_0^d \frac{J_p(x)}{J_p(d)} e^{[E_c(x)-E_c(d)]/kT} dx]} (e^{\Delta E_{Fn}/kT} - 1), \quad \text{(A5)}$$

where $\Delta E_{Fn} = E_{Fn}(0) - E_{Fn}(d)$. [Equation (A5) is obtained by multiplying Eq. (A3) with $e^{[E_c(0)-E_c(d)]/kT}$, noting that $J_n(x) = J_n(d)[J_p(x)/J_p(d)]$ at $V = V_{\rm OC}$, and solving for $J_n(d)$.]

In the case when recombination dominates well within the bulk, only electrons and holes that are sufficiently close to the cathode are able to leave the active layer and recombine at the surface. In this case, due to the perfectly selective anode ($S_n = 0$), we expect $\Delta E_{Fn} = q(V_{\rm OC,max} - V_{\rm OC})$, where $V_{\rm OC,max}$ is given by Eq. (10).

a. $S_p \gg v_{p,d}$

With the approximation that all holes within a distance L_n^* from the cathode are able to avoid recombination in the bulk, while the rest recombine in the bulk, Eq. (3) reveals

$$J_p(x) \approx \begin{cases} qG_L(x - d + L_n^*) & \text{when } d - L_n^* < x \le d \\ 0 & \text{otherwise.} \end{cases} \quad \text{(A6)}$$

Close to flatband conditions, we have that $E_c(0) \approx E_c(d)$. In this case,

$$J_n(d) \approx -\frac{2kT\mu_n n_{\rm cat}}{L_n^*} (e^{\Delta E_{Fn}/kT} - 1), \quad \text{(A7)}$$

while the open-circuit voltage approaches $qV_{\rm OC} \to E_g - \varphi_{\rm cat} - kT \ln(2\mu_p kT N_v / qG_L L_n^{*2})$. In conjunction with Eq. (10), we obtain $\Delta E_{Fn} = kT \ln(2\mu_p kT / q\beta n_{\rm cat} L_n^{*2})$. Inserting into Eq. (A7), it follows from the open-circuit condition $-J_n(d) = J_p(d) = qGL_n^*$ that

$$L_n^* \approx \left(\frac{\mu_{\rm eff} kT}{q\sqrt{\beta_R G_L}}\right)^{1/2}, \quad \text{(A8)}$$

where $\mu_{\rm eff} = 2\sqrt{\mu_p \mu_n}$.

b. $S_p \ll v_{p,d}$

In the following, we assume the requirements (i) $S_p \ll v_{p,d}$ and (ii) $L_n^{**} \ll d$ to be valid. Under conditions of $p \gg n$ and constant E_{Fp} throughout the active layer, the upward bending of $E_c(x)$ close to the cathode, as obtained from the Poisson equation, is given by

$$E_c(x) \approx E_c(d) - 2kT \ln\left(1 + \frac{d - x}{L_{\rm sc}}\right), \quad \text{(A9)}$$

where $L_{\rm sc} \equiv \sqrt{2\varepsilon\varepsilon_0 kT/q^2 p(d)}$. Then, if we effectively approximate the decrease in R [from $R \approx G_L$ to $R(d) = \beta_R n_{\rm cat} p(d)$] to be linear within the region $x \in [d - 2L_n^{**}, d]$, we find $J_p(d) = q[G_L - \beta_R n_{\rm cat} p(d)] L_n^{**}$. With $G - R \approx [G_L - \beta_R n_{\rm cat} p(d)][(x - d + 2L_n^{**})/2L_n^{**}]$ for $x > d - 2L_n^{**}$, and $J_p(x) \approx 0$ otherwise, we obtain $J_p(x) = J_p(d)[(x - d + 2L_n^{**})/2L_n^{**}]^2$. Accordingly, the integral $B_n = \int_0^d [J_p(x)/J_p(d)] e^{[E_c(x)-E_c(d)]/kT} dx$ in Eq. (A5) can be evaluated as

$$B_n = \int_{d-2L_n^{**}}^{d} \left(\frac{x-d+2L_n^{**}}{2L_n^{**}}\right)^2 \left(1+\frac{d-x}{L_{sc}}\right)^{-2} dx$$
$$= -L_{sc} + L_{sc}\left(2+\frac{L_{sc}}{L_n^{**}}\right)\left[1-\frac{L_{sc}}{2L_n^{**}}\ln\left(1+\frac{2L_n^{**}}{L_{sc}}\right)\right]$$
$$\approx L_n^{**}\left(1+\frac{L_n^{**}}{L_{sc}}\right)^{-1}, \quad \text{(A10)}$$

where the approximation $\{1-[\ln(1+u)/u]\} \approx (1-\{1/[1+(u/2)]\})$ was used in the last step. This purely mathematical approximation is exact in the limits of small and large $u = 2L_n^{**}/L_{sc}$, while a deviation of roughly 5% to 10% is found at moderate u.

Now, utilizing Eq. (22), we can write $\Delta E_{Fn} = kT\ln[G_L p_{cat}/\beta_R n_i^2 p(d)] = kT\ln[G_L/\beta_R n_{cat} p(d)]$; inserting into Eq. (A5), in conjunction with Eq. (A10), we obtain

$$J_n(d) \approx -(\mu_n kT n_{cat}/\{L_n^{**}[1+(L_n^{**}/L_{sc})]^{-1}\}) \times \{[G_L/\beta_R n_{cat} p(d)]-1\}$$
$$= -(\{\mu_n kT[G_L - \beta_R n_{cat} p(d)]\}/ \{\beta_R p(d) L_n^{**}[1+(L_n^{**}/L_{sc})]^{-1}\}).$$

Then, noting that $J_n(d) = -q[G_L - \beta_R n_{cat} p(d)]L_n^{**}$ and solving for L_n^{**} reveals

$$L_n^{**} \approx \frac{\mu_n}{\beta_R}\sqrt{\frac{kT}{8\varepsilon\varepsilon_0 p(d)}}\left(\sqrt{1+\frac{8\varepsilon\varepsilon_0\beta_R}{q\mu_n}}+1\right), \quad \text{(A11)}$$

or equivalently, $L_n^{**} = [K^{-1}/\sqrt{p(d)}]$ with K defined by Eq. (24).

The above analysis is valid for $L_n^{**} \ll d$ only. At large mobilities and small β_R, however, when L_n^{**} becomes comparable to d, conditions similar to Eq. (14) with $R \sim$ const are approached. Thus, we expect $J_p(d) = q[G_L - \beta_R n_{cat} p(d)]d_{eff}$, where $d_{eff} = L_n^{**}$ when $L_n^{**} \ll d$, and $d_{eff} = d$ when $L_n^{**} \gg d$. Equating with Eq. (11), we finally arrive at Eq. (23).

APPENDIX B: THE DEVICE MODEL

A previously developed numerical drift-diffusion model, as described in Ref. [27], is used for the macroscopic simulations. Macroscopic device models of this kind have been particularly successful in describing the electrical behavior of both inorganic and organic-based devices and is in this sense very general [5,21,39]. The model solves the continuity equations coupled to the drift-diffusion equations, in conjunction with the Poisson equation. The default parameters used in the simulations are given in Table I. In the case of Ohmic contact for holes at the anode and electrons at the cathode, we assume $p_{an} = N_v$ and $n_{cat} = N_c$, respectively. Furthermore, additional leakage currents (due to parasitic shunt resistances) are assumed to be zero.

TABLE I. Input parameters in the numerical model. Unless otherwise stated these parameters are used in the simulations.

E_g	1.2 eV
T	300 K
ε	3.5
d	150 nm
N_c, N_v	10^{26} cm^{-3}
μ_n, μ_p	5×10^{-3} cm^2 V^{-1} s^{-1}
G_L at 1 sun	6.24×10^{21} cm^{-3} s^{-1}

[1] C. Deibel and V. Dyakonov, Polymer-fullerene bulk heterojunction solar cells, Rep. Prog. Phys. **73**, 096401 (2010).
[2] L. Dou, J. You, Z. Hong, Z. Xu, G. Li, R. A. Street, and Y. Yang, 25th anniversary article: A decade of organic/polymeric photovoltaic research, Adv. Mater. **25**, 6642 (2013).
[3] N.-G. Park, Perovskite solar cells: An emerging photovoltaic technology, Mater. Today **18**, 65 (2015).
[4] Mohammad Khaja Nazeeruddin, and Henry Snaith, Methylammonium lead triiodide perovskite solar cells: A new paradigm in photovoltaics, MRS Bull. **40**, 641 (2015).
[5] T. Kirchartz, J. Bisquert, I. Mora-Sero, and G. Garcia-Belmonte, Classification of solar cells according to mechanisms of charge separation and charge collection, Phys. Chem. Chem. Phys. **17**, 4007 (2015).
[6] L. J. A. Koster, V. D. Mihailetchi, R. Ramaker, and P. W. M. Blom, Light intensity dependence of open-circuit voltage of polymer:fullerene solar cells, Appl. Phys. Lett. **86**, 123509 (2005).
[7] T. Kirchartz, J. Mattheis, and U. Rau, Detailed balance theory of excitonic and bulk heterojunction solar cells, Phys. Rev. B **78**, 235320 (2008).
[8] K. Vandewal, K. Tvingstedt, A. Gadisa, O. Inganäs, and J. V. Manca, On the origin of the open-circuit voltage of polymer-fullerene solar cells, Nat. Mater. **8**, 904 (2009).
[9] J. C. Blakesley and D. Neher, Relationship between energetic disorder and open-circuit voltage in bulk heterojunction organic solar cells, Phys. Rev. B **84**, 075210 (2011).
[10] W. Tress, K. Leo, and M. Riede, Optimum mobility, contact properties, and open-circuit voltage of organic solar cells: A drift-diffusion simulation study, Phys. Rev. B **85**, 155201 (2012).
[11] K. R. Graham, P. Erwin, D. Nordlund, K. Vandewal, R. Li, G. O. Ngongang Ndjawa, E. T. Hoke, A. Salleo, M. E. Thompson, M. D. McGehee, and A. Amassian, Re-evaluating the role of sterics and electronic coupling in determining the open-circuit voltage of organic solar cells, Adv. Mater. **25**, 6076 (2013).
[12] Q. Bao, O. Sandberg, D. Dagnelund, S. Sanden, S. Braun, H. Aarnio, X. Liu, W. Chen, R. Osterbacka, and M. Fahlman, Trap-assisted recombination via integer charge transfer states in organic bulk heterojunction photovoltaics, Adv. Funct. Mater. **24**, 6309 (2014).
[13] W. Yang, Y. Yao, and C.-Q. Wu, Origin of the high open circuit voltage in planar heterojunction perovskite solar

cells: Role of the reduced bimolecular recombination, J. Appl. Phys. **117**, 095502 (2015).

[14] J. Yao, T. Kirchartz, M. S. Vezie, M. A. Faist, W. Gong, Z. He, H. Wu, J. Troughton, T. Watson, D. Bryant, and J. Nelson, Quantifying Losses in Open-Circuit Voltage in Solution-Processable Solar Cells, Phys. Rev. Applied **4**, 014020 (2015).

[15] N. K. Elumalai and Ashraf Uddin, Open circuit voltage of organic solar cells: An in-depth review, Energy Environ. Sci. **9**, 391 (2016).

[16] T. Kirchartz, B. E. Pieters, K. Taretto, and U. Rau, Mobility dependent efficiencies of organic bulk heterojunction solar cells: Surface recombination and charge transfer state distribution, Phys. Rev. B **80**, 035334 (2009).

[17] T. Kirchartz, F. Deledalle, P. Shakya Tuladhar, J. R. Durrant, and J. Nelson, On the differences between dark and light ideality factor in polymer:fullerene solar cells, Phys. Chem. Lett. **4**, 2371 (2013).

[18] T. Kirchartz, B. E. Pieters, J. Kirkpatrick, U. Rau, and J. Nelson, Recombination via tail states in polythiophene: fullerene solar cells, Phys. Rev. B **83**, 115209 (2011).

[19] T. Kirchartz and J. Nelson, Meaning of reaction orders in polymer:fullerene solar cells, Phys. Rev. B **86**, 165201 (2012).

[20] M. Nyman, O. J. Sandberg, and R. Österbacka, 2D and trap-assisted 2D Langevin recombination in polymer:fullerene blends, Adv. Energy Mater. **5**, 1400890 (2015).

[21] P. Würfel, *Physics of Solar Cells*, 2nd ed. (Wiley-VCH, Weinheim, Germany, 2009).

[22] G. A. H. Wetzelaer, M. Kuik, M. Lenes, and P. W. M. Blom, Origin of the dark-current ideality factor in polymer: fullerene bulk heterojunction solar cells, Appl. Phys. Lett. **99**, 153506 (2011).

[23] W. Tress, K. Leo, and M. Riede, Dominating recombination mechanisms in organic solar cells based on ZnPc and C60, Appl. Phys. Lett. **102**, 163901 (2013).

[24] C. J. Brabec, A. Cravino, D. Meissner, N. S. Sariciftci, T. Fromherz, M. T. Rispens, L. Sanchez, and J. C. Hummelen, Origin of the open circuit voltage of plastic solar cells, Adv. Funct. Mater. **11**, 374 (2001).

[25] E. J. Juarez-Perez, M. Wussler, F. Fabregat-Santiago, K. Lakus-Wollny, E. Mankel, T. Mayer, W. Jaegermann, and I. Mora-Sero, Role of the selective contacts in the performance of lead halide perovskite solar cells, J. Phys. Chem. Lett. **5**, 680 (2014).

[26] V. D. Mihailetchi, P. W. M. Blom, J. C. Hummelen, and M. T. Rispens, Cathode dependence of the open-circuit voltage of polymer:fullerene bulk heterojunction solar cells, J. Appl. Phys. **94**, 6849 (2003).

[27] O. J. Sandberg, M. Nyman, and R. Österbacka, Effect of Contacts in Organic Bulk Heterojunction Solar Cells, Phys. Rev. Applied **1**, 024003 (2014).

[28] D. Rauh, A. Wagenpfahl, C. Deibel, and V. Dyakonov, Relation of open circuit voltage to charge carrier density in organic bulk heterojunction solar cells, Appl. Phys. Lett. **98**, 133301 (2011).

[29] R. Sokel and R. C. Hughes, Numerical analysis of transient photoconductivity in insulators, J. Appl. Phys. **53**, 7414 (1982).

[30] Y. Zhou, J. W. Shim, C. F. Hernanderz, A. Sharma, K. A. Knauer, A. J. Giordano, S. R. Marder, and B. Kippelen, Direct correlation between work function of indium-tin-oxide electrodes and solar cell performance influenced by ultraviolet irradiation and air exposure, Phys. Chem. Chem. Phys. **14**, 12014 (2012).

[31] J. Reinhardt, M. Grein, C. Bühler, M. Schubert, and U. Würfel, Identifying the impact of surface recombination at electrodes in organic solar cells by means of electroluminescence and modeling, Adv. Energy Mater. **4**, 1400081 (2014).

[32] A. Zampetti, A. H. Fallahpour, M. Dianetti, L. Salamandra, F. Santoni, A. Gagliardi, M. Auf der Maur, F. Brunetti, A. Reale, T. M. Brown, and A. Di Carlo, Influence of the interface material layers and semiconductor energetic disorder on the open circuit voltage in polymer solar cells, J. Polym. Sci. B **53**, 690 (2015).

[33] S. Wheeler, F. Deledalle, N. Tokmoldin, T. Kirchartz, J. Nelson, and J. R. Durrant, Influence of Surface Recombination on Charge-Carrier Kinetics in Organic Bulk Heterojunction Solar Cells with Nickel Oxide Interlayers, Phys. Rev. Applied **4**, 024020 (2015).

[34] A. Wagenpfahl, C. Deibel, and V. Dyakonov, Organic solar cell efficiencies under the aspect of reduced surface recombination velocities, IEEE J. Sel. Top. Quantum Electron. **16**, 1759 (2010).

[35] E. Ahlswede, J. Hanisch, and M. Powalla, Comparative study of the influence of LiF, NaF, and KF on the performance of polymer bulk heterojunction solar cells, Appl. Phys. Lett. **90**, 163504 (2007).

[36] Z. C. He, C. M. Zhong, X. Huang, W. Y. Wong, H. B. Wu, L. W. Chen, S. J. Su, and Y. Cao, Simultaneous enhancement of open-circuit voltage, short-circuit current density, and fill factor in polymer solar cells, Adv. Mater. **23**, 4636 (2011).

[37] E. L. Ratcliff, A. Garcia, S. A. Paniagua, S. R. Cowan, A. J. Giordano, D. S. Ginley, S. R. Marder, J. J. Berry, and D. C. Olson, Investigating the influence of interfacial contact properties on open circuit voltages in organic photovoltaic performance: Work function versus selectivity, Adv. Energy Mater. **3**, 647 (2013).

[38] H. Wang, E. D. Gomez, Z. Guan, C. Jaye, M. F. Toney, D. A. Fischer, A. Kahn, and Y.-L. Loo, Tuning contact recombination and open-circuit voltage in polymer solar cells via self-assembled monolayer adsorption at the organic-metal oxide interface, J. Phys. Chem. C **117**, 20474 (2013).

[39] S. M. Sze, *Physics of Semiconductor Devices* (Wiley & Sons, New York, 1981).

[40] G. A. H. Wetzelaer, L. J. A. Koster, and P. W. M. Blom, Validity of the Einstein Relation in Disordered Organic Semiconductors, Phys. Rev. Lett. **107**, 066605 (2011).

[41] J. C. Blakesley and N. C. Greenham, Charge transfer at polymer-electrode interfaces: The effect of energetic disorder and thermal injection on band bending and open-circuit voltage, J. Appl. Phys. **106**, 034507 (2009).

[42] M. Kuik, L. J. A. Koster, G. A. H. Wetzelaer, and P. W. M. Blom, Trap-Assisted Recombination in Disordered Organic Semiconductors, Phys. Rev. Lett. **107**, 256805 (2011).

[43] A. Pivrikas, G. Juška, A. J. Mozer, M. Scharber, K. Arlauskas, N. S. Sariciftci, H. Stubb, and R. Österbacka,

Bimolecular Recombination Coefficient as a Sensitive Testing Parameter for Low-Mobility Solar-Cell Materials, Phys. Rev. Lett. **94**, 176806 (2005).

[44] C. Groves and N. C. Greenham, Bimolecular recombination in polymer electronic devices, Phys. Rev. B **78**, 155205 (2008).

[45] M. C. Heiber, C. Baumbach, V. Dyakonov, and C. Deibel, Encounter-Limited Charge-Carrier Recombination in Phase-Separated Organic Semiconductor Blends, Phys. Rev. Lett. **114**, 136602 (2015).

[46] D. H. K. Murthy, A. Melianas, Z. Tang, G. Juska, K. Arlauskas, F. Zhang, L. D. A. Siebbeles, O. Inganäs, and T. J. Savenije, Origin of reduced bimolecular recombination in blends of conjugated polymers and fullerenes, Adv. Funct. Mater. **23**, 4262 (2013).

[47] G. A. H. Wetzelaer, N. J. Van der Kaap, L. J. A. Koster, and P. W. M. Blom, Quantifying bimolecular recombination in organic solar cells in steady state, Adv. Energy Mater. **3**, 1130 (2013).

[48] C. Wehrenfennig, G. E. Eperon, M. B. Johnston, H. J. Snaith, and L. M. Herz, High charge carrier mobilities and lifetimes in organolead trihalide perovskites, Adv. Mater. **26**, 1584 (2014).

[49] J. C. Scott and G. C. Malliaras, Charge injection and recombination at the metal-organic interface, Chem. Phys. Lett. **299**, 115 (1999).

[50] P. de Bruyn, A. H. P. van Rest, G. A. H. Wetzelaer, D. M. de Leeuw, and P. W. M. Blom, Diffusion-Limited Current in Organic Metal-Insulator-Metal Diodes, Phys. Rev. Lett. **111**, 186801 (2013).

[51] P. Nelson, *Biological Physics: Energy, Information, Life* (W. H. Freeman Co. Ltd, New York, 2004), pp. 260–272, 283–289.

[52] For Ohmic contacts we require $L_{\mathrm{cat}} \ll d$ and $\alpha = \sqrt{n_{\mathrm{ph}}/n_{\mathrm{cat}}} \ll 1$; Eq. (12) reduces to $v_{d,p} = (\mu_p kT/q)B_p^{-1}$ with $B_p = \alpha^2 \int_0^d [(2x/d) - 1]\coth^2\{[1 + ([d-x]/L_{\mathrm{cat}})]\alpha\}\, dx \approx L_{\mathrm{cat}}$, where $\coth(u) \approx 1/u$ (for $u \ll 1$) and $\coth(u) \to 1$ (for $u \gg 1$) have been utilized.

[53] S. Schäfer, A. Petersen, T. A. Wagner, R. Kniprath, D. Lingenfelser, A. Zen, T. Kirchartz, B. Zimmermann, U. Wurfel, X. Feng, and T. Mayer, Influence of the indium tin oxide/organic interface on open-circuit voltage, recombination, and cell degradation in organic small-molecule solar cells, Phys. Rev. B **83**, 165311 (2011).

[54] M. Lu, P. de Bruyn, H. T. Nicolai, G.-J. A. Wetzelaer, and P. W. Blom, Hole-enhanced electron injection from ZnO in inverted polymer light-emitting diodes, Org. Electron. **13**, 1693 (2012).

[55] A. Sundqvist, O. J. Sandberg, M. Nyman, J-H. Smått, and R. Österbacka, Origin of the S-shaped JV curve and the light-soaking issue in inverted organic solar cells, Adv. Energy Mater. **6**, 1502265 (2016).

[56] Now, with $J_p(x)$ given by Eq. (A6), Eq. (12) reveals $v_{d,p} = \mu_p F[(kT/qFL_n^*)(e^{qFL_n^*/kT} - 1) - 1]^{-1} \approx [(2\mu_p kT/L_n^*) - (2\mu_p F/3)]$, where $-qFL_n^* \ll kT$ was assumed in the last step. Then, from Eq. (11), with $J_p(d) = qG_L L_n^*$, Eq. (20) follows.

[57] Equating Eqs. (7a) and (11) at $V = V_{\mathrm{OC}}$ yields $p(d) = \{p_{\mathrm{cat}}/[1 + (S_p/v_{d,p})]\}(e^{qV_{\mathrm{OC}}/kT} - 1) + p_{\mathrm{cat}} \approx p_{\mathrm{cat}} e^{qV_{\mathrm{OC}}/kT}$, for $S_p \ll v_{d,p}$, while $p(d) \to p_{\mathrm{cat}}$ when $S_p \to \infty$.

[58] For $R = \beta_R(p)p^2 \propto p^\alpha$, $\beta_R(p)$ is also dependent on G_L; in this case the ratio (G_L/β_R) becomes equal to $(G_L/\gamma)^{m_R}$ in Eq. (10), where γ is a coefficient independent of G_L.

[59] V. Gupta, A. K. K. Kyaw, D. H. Wang, S. Chand, G. C. Bazan, and A. J. Heeger, Barium: An efficient cathode layer for bulk-heterojunction solar cells, Sci. Rep. **3**, 1965 (2013).